Check for updates

ChemSusChem

Research Article
doi.org/10.1002/cssc.202402378

Chemistry Europe
European Chemical Societies Publishing

www.chemsuschem.org

Gold–Indium Electrocatalysts for the Selective Oxidation of Glycerol Coupled with CO_2 Reduction

Martí Molera, Kevin Fernández-Caso, Mohamed Amazian, Guillermo Díaz-Sainz, José Solla-Gullón, Manuel Álvarez-Guerra,* Maria Sarret, and Teresa Andreu*

Glycerol electrooxidation is a promising alternative to the oxygen evolution reaction in carbon dioxide electroreduction processes. It has the potential to both reduce the overall cell voltage and enable the commercialization of anodic oxidation products. Gold is a material that exhibits a high performance for glycerol oxidation but has a high manufacturing cost. In this work, a gold indium alloy has been synthesized that exhibits enhanced electrocatalytically properties, as evidenced by a reduction in the glycerol oxidation onset potential by 210 mV while reducing the electrode cost by 28%. This electrocatalyst has been evaluated in a flow cell configuration coupled with the cathodic reduction of carbon dioxide, and high faradaic efficiencies of up to 90% have been achieved for both the anodic and cathodic products.

1. Introduction

The production of glycerol from the biodiesel industry has seen a significant increase in recent years, reaching a point where it has exceeded the market demand. Consequently, the price of glycerol has declined to 0.80 € $kg^{-1}$and 0.52 € kg^{-1} for crude and refined glycerol respectively.[1] Recently, glycerol oxidation reaction (GOR) has emerged as a promising alternative to the oxygen evolution reaction (OER). This is due to the fact that GOR exhibits faster kinetics and lower oxidation potential, which could offer significant advantages in terms of energy efficiency.[2,3]

Furthermore, this reaction produces a diverse range of organic compounds with high added value, like dihydroxyacetone and formic acid, among others. These compounds facilitate the commercialization of the anodic process, thereby providing an industrial application for glycerol.[4–6] Similarly to the OER, the GOR is employed in conjunction with the hydrogen evolution reaction (HER) to produce hydrogen, or the CO_2 reduction reaction (CO_2RR) to produce valuable chemicals by using renewable energies.[7–9] This process is of particular interest as it can enable a coelectrolysis process, whereby low-C products are produced in both the GOR and CO_2RR reactions,[10,11] thereby contributing to the circular economy.

Gold has been employed as a conventional catalyst for glycerol oxidation by depositing Au nanoparticles over ceramic substrates due to its high affinity for CO oxidation which mitigates the issue of CO poisoning.[12–14] Additionally, gold can be employed as an electrocatalyst through electrodeposition of a thin gold layer[15,16] or deposition of nanoparticles onto conductive substrates, such as carbon structures.[17] These deposited nanoparticles can be synthesized in a variety of structures, including nanoflowers,[18] nanowires,[19,20] or nanosheets.[21]

The use of these electrocatalysts in controlled glycerol electrolysis has been demonstrated to yield high faradaic efficiencies (FE), resulting in the production of three main products: formate, glycerate, and glycolate.[22] However, the use of lower potentials has been shown to facilitate the generation of less oxidized products, like dihydroxyacetone, glyceraldehyde, and lactate.[23]

Despite the favorable performance of gold in glycerol oxidation, its elevated market cost significantly increases the expense of the electrocatalyst. As a result, it has been combined with other metals, including platinum (Pt),[23] palladium (Pd),[24,25] and silver (Ag),[26] with the aim of enhancing its electrocatalytic properties. This has been achieved by increasing the number of active sites and modifying the electronic structure of the catalyst surface. Another suitable metal for alloying with gold is indium, being less expensive than noble metals. Gold–indium alloys have been widely used for low-temperature soldering, but have received little attention as electrocatalysts. However, incorporating indium into Pt or Pd electrocatalysts has proven effective for electrooxidation reactions by shifting the d-band center, facilitating alcohol adsorption, and mitigating CO poisoning.[27–29] In this work, a

M. Molera, M. Amazian, M. Sarret, T. Andreu
Sustainable Electrochemical Processes
Department of Materials Science and Physical Chemistry & Institute of Nanoscience and Nanotechnology (IN2UB)
Facultat de Química
Universitat de Barcelona
Martí i Franquès, 1-11, 08028 Barcelona, Spain
E-mail: tandreu@ub.edu

K. Fernández-Caso, G. Díaz-Sainz, M. Álvarez-Guerra
Departamento de Ingenierías Química y Biomolecular
Universidad de Cantabria
Avda. Los Castros, s/n, 39005 Santander, Spain
E-mail: manuel.alvarezg@unican.es

J. Solla-Gullón
Instituto de Electroquímica
Universidad de Alicante
Apdo. 99, E-03080 Alicante, Spain

Supporting information for this article is available on the WWW under https://doi.org/10.1002/cssc.202402378

© 2025 The Author(s). ChemSusChem published by Wiley-VCH GmbH. This is an open access article under the terms of the Creative Commons Attribution-NonCommercial-NoDerivs License, which permits use and distribution in any medium, provided the original work is properly cited, the use is non-commercial and no modifications or adaptations are made.

© 2025 The Author(s). ChemSusChem published by Wiley-VCH GmbH

novel gold–indium alloy was electrodeposited over a nickel foam substrate, resulting in enhanced gold electrocatalytic properties for glycerol oxidation while reducing the cost of the electrocatalyst. This newly developed alloy has been implemented in a flow cell setup, which has demonstrated great FE in GOR coupled to CO_2RR, in a covalorization approach.

2. Results and Discussion

2.1. Electrode Characterization

Figure 1 and S1, Supporting Information, illustrate the morphologies of Au and AuIn electrodeposited on nickel foams. As shown in the field emission scanning electron microscopy (FESEM) images, the Au electrode exhibits a plain yet rough morphology with perpendicular laminar sheets, while the AuIn electrode displays a rough cauliflower morphology. The double-layer capacitance measurement (Figure S2, Supporting Information) reveals that AuIn has a surface area about 19 times higher than Au and about 630 times higher than the Ni-foam support (Table S1, Supporting Information). The energy-dispersive spectroscopy (EDS) analysis (Table S2, Supporting Information) indicates that Au is composed of 100% gold, while AuIn has a 72% gold and 28% indium weight composition. This indicates that the AuIn catalyst cost is ≈50.4 € g^{-1}, representing a 28% reduction in cost compared to the Au catalyst (Table S3, Supporting Information).

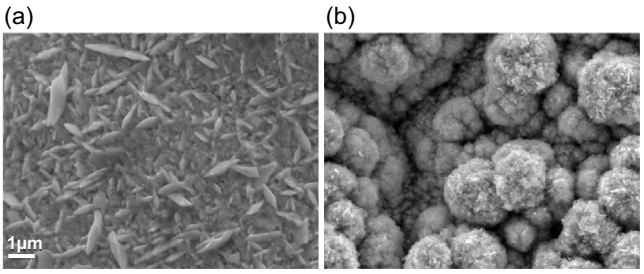

Figure 1. FESEM images of the a) Au and b) AuIn electrodes.

As illustrated in **Figure 2**a, the X-ray diffraction (XRD) analysis reveals the presence of Ni foam support (JCPDS 00-004-0850) for both electrodes. The XRD analysis of Au confirms the electrodeposition of a gold layer, as indicated by the presence of the cubic structure of gold (JCPDS 01-089-3697) peaks. The AuIn diffractogram shows that gold peaks have broadened and their intensity has decreased. This indicates a reduction in crystallinity, which correlates with the increased roughness of the electrode. Furthermore, additional broad peaks have been identified between 34° and 42°.

As illustrated in Figure 2b, the observed peaks can be attributed to two distinct AuIn phases (JCPDS 00-010-0211 and 00-029-0647). However, the highly broad peaks may indicate that the AuIn alloy does not have a precise composition. The X-ray photoelectronic spectroscopy (XPS) analysis of the Au electrode (Figure S3, Supporting Information) reveals the presence of the Au $4f_{7/2}$ and Au $4f_{5/2}$ peaks at 83.8 and 87.5 eV, respectively. This indicates that the electrodeposited gold is in its metallic state. The XPS analysis of the AuIn (Figure 2c,d) also demonstrates

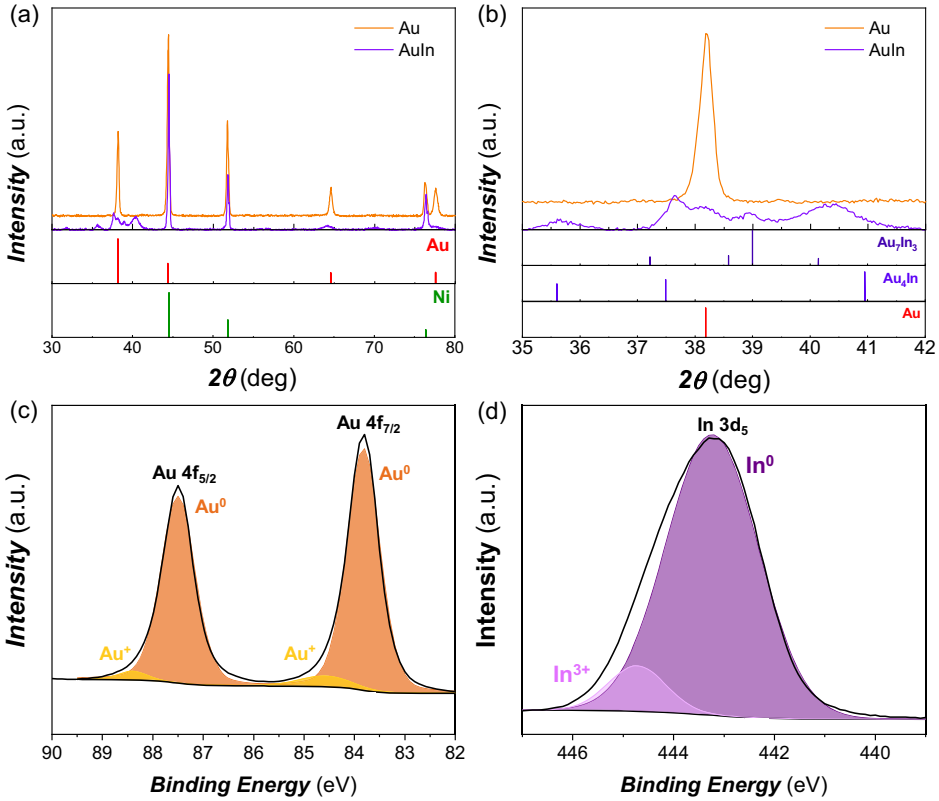

Figure 2. XRD patterns of a) Au and b) AuIn electrodes. XPS spectra of c,d) AuIn electrode.

© 2025 The Author(s). ChemSusChem published by Wiley-VCH GmbH

1864564x, 2025, 12, Downloaded from https://chemistry-europe.onlinelibrary.wiley.com/doi/10.1002/cssc.202402378 by Universidad De Cantabria, Wiley Online Library on [07/07/2025]. See the Terms and Conditions (https://onlinelibrary.wiley.com/terms-and-conditions) on Wiley Online Library for rules of use; OA articles are governed by the applicable Creative Commons License

the presence of the Au $4f_{7/2}$ and Au $4f_{5/2}$ peaks, as well as the In $3d_5$ peak at 443.4 eV. This confirms that both metals are in the metallic state, with the additional peaks on the left of the main peak corresponding to surface oxides.

2.2. Electrochemical Characterization

Figure 3 illustrates the cyclic voltammetry measurements of Au and AuIn electrodes. For the OER, both electrodes exhibit a high overpotential, which suggests that there is no competition between the GOR and the OER at low electrode potentials. With regard to the GOR, a distinctive shape can be discerned. As illustrated, in the anodic scan at 1.3–1.5 V_{RHE}, the current density decreases before exhibiting a rise at higher potentials. When the scan is reversed to cathodic potentials, at 1.25 V_{RHE} there is a sudden spike in intensity, followed by an increase in intensity value that approaches those of the anodic scan. This phenomenon can be attributed to the oxidation of metallic gold to gold (III) at about 1.3V_{RHE}, as illustrated in Figure S4, Supporting Information. This process results in the deactivation of the surface, which presents a higher GOR potential. Subsequently, during the cathodic scan, the material is reduced back to metallic gold at 1.25 V_{RHE}, thereby reactivating the surface.[21,30] The Au electrode has an onset potential of 0.85 V_{RHE} and reaches a 160 mA cm^{-2} intensity peak in the anodic scan, while in the cathodic it has a peak of 260 mA cm^{-2}. The AuIn electrode has a lower onset potential of 0.64 V_{RHE} and its anodic and cathodic scan peaks are also higher, reaching values of 240 and 400 mA cm^{-2} respectively. In contrast, metallic indium is inactive in this potential range, with an onset potential of 1.41 V_{RHE}. These findings point out that the AuIn electrode shows a reduction of 0.21 V in onset potential, indicating that indium enhances the electrocatalytic properties of gold, enabling glycerol oxidation at lower potentials.

2.3. Glycerol Electrolysis

To analyze the product distribution of the GOR, we conducted electrolysis in a single-compartment three-electrode electrochemical cell in galvanostatic conditions. As illustrated in **Figure 4**, Au and AuIn electrodes exhibit high overall FE (≈90%). In these conditions, AuIn exhibits an electrode potential of 0.85 V_{RHE}, while for Au it is 1.1 V_{RHE} (Figure S5, Supporting Information). This further highlights the enhanced electrocatalytic performance of the AuIn electrode. Regarding the product distribution, both electrodes yield the same oxidation products, namely glycerate, glycolate, formate, dihydroxyacetone, lactate, and pyruvate. The two electrodes present small differences in product distribution, as anticipated from the CV measurements. AuIn enhances the formation of C3 products (dihydroxyacetone and glycerate), increasing the FE toward them from 25 to 42%. Meanwhile, Au favors the production of C2 and C1 products (glycolate and formate), as their production is increased from 33 to 37% for C2 and from 16 to 24 for C1. These results show that the AuIn electrode reduces the reaction potential while enhancing the electrocatalytic properties of bare Au, as evidenced by the enhanced production of less oxidized products.

2.4. Oxidation of Intermediate Products

Given that the oxidation of glycerol was conducted in a basic medium, chemical reactions can occur simultaneously, particularly the degradation of dihydroxyacetone via Cannizzaro rearrangement.[31,32] So, we conducted additional electrolysis in order to discern the effect of chemical degradation and achieve a better understanding of the reaction pathways. These electrolysis were conducted for different intermediate products in divided H-type cells, to eliminate any effects of the cathodic reaction, as well as to observe if there was any product reduction. Because of that both the anodic and cathodic compartments were analyzed. Additionally, some electrolyte was kept outside the H cell, in basic

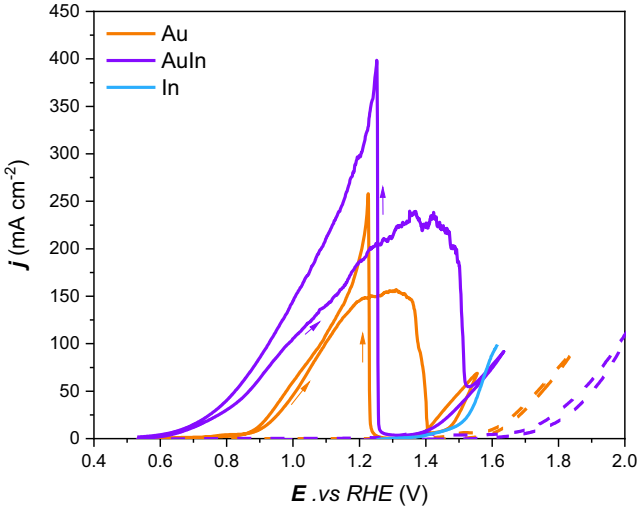

Figure 3. Cyclic voltammetry measurements recorded at a scan rate of 2 mV s^{-1} in KOH 1 M (dotted line) and KOH 1 M and glycerol 0.1 M (continuous line).

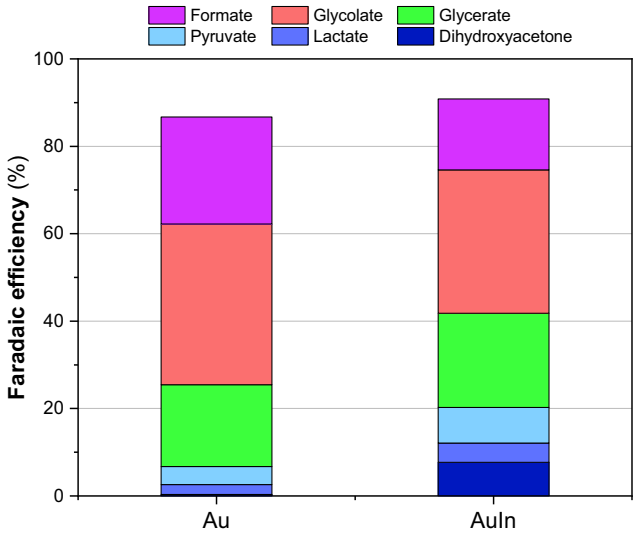

Figure 4. FE for glycerol oxidation in batch electrolysis of 5 mL of KOH 1 M and glycerol 0.1 M solution, at a current of 41.6 mA cm^{-2} and a charge of 5 C mL^{-1}.

© 2025 The Author(s). ChemSusChem published by Wiley-VCH GmbH

18645564x, 2025, 12, Downloaded from https://chemistry-europe.onlinelibrary.wiley.com/doi/10.1002/cssc.202402378 by Universidad De Cantabria, Wiley Online Library on [07/07/2025]. See the Terms and Conditions (https://onlinelibrary.wiley.com/terms-and-conditions) on Wiley Online Library for rules of use; OA articles are governed by the applicable Creative Commons License

media, to let the intermediates chemically degrade. After the electrolysis ended, all the 3 samples were acidified to stop the chemical degradation. The results for the Au electrode are presented in Table S4, Supporting Information, and the results for AuIn are provided in Table S5, Supporting Information.

First, dihydroxyacetone and glyceraldehyde electrolysis were carried out, as they are the products of the first glycerol oxidation step. Glyceraldehyde is produced when the terminal alcohol is oxidized and dihydroxyacetone when the central one is oxidized. Dihydroxyacetone electrolysis yields lactate, glycolate, and formate as major compounds and acetate in trace amounts (**Figure 5**a). The concentration of lactate is similar to the nonelectrolyzed sample, indicating that lactate is formed via the Cannizzaro degradation mechanism. Similarly, glyceraldehyde electrolysis (Figure 5b) also produces lactate via Cannizzaro. This is due to the fact that both compounds are in an equilibrium mediated by OH^-.[33,34] Glyceraldehyde electrolysis also yields glycolate and formate because independently of the mother molecule, the C—C cleavage will yield these two products as can be seen in Figure S6, Supporting Information. Furthermore, glyceraldehyde electrolysis also produces glycerate, as it can only be formed by the direct oxidation of the aldehyde.[35,36]

After the glyceraldehyde electrolysis, we proceeded to oxidize glycerate (Figure 5c), as it is an exclusive product of its reaction pathway. This electrolysis yielded formate as well as glycolate. However, this second product is exclusively produced by chemical degradation since it is also present in the nonelectrolyzed sample. This suggests that the glycerate C—C bonds are cleaved simultaneously, resulting in the formation of three formate molecules. However, unlike the chemical degradation of dihydroxyacetone, only about 8% of glycerate degrades into glycolate, concluding that glycerate is fairly stable and only a small percentage of the detected glycolate will come from chemical degradation.

Then, we considered glycolate and formate for the electrolysis, as they are the shared products of dihydroxyacetone and glyceraldehyde electrolysis. Glycolate electrolysis (Figure 5d) only yielded formate, but we can assume that complete oxidation to CO_2 also takes place. Considering the glycolate consumption and the analyzed products formed (formate), we can only justify 40% of the charge passed. We can therefore attribute the remaining charge to water oxidation (OER). This indicates that glycolate oxidation is an unfavored reaction and could explain its high production on glycerol electrolysis. In the formate electrolysis, we observed a similar effect, as less than 20% of the electrons were used for formate oxidation. This indicates that this oxidation is even more unfavorable, and thus, there will be minimal oxidation to CO_2 in the overall process, as formate is the final molecule in all reaction pathways.

Finally, we conducted lactate electrolysis (Figure 5e). Here, the product distribution differs significantly from previous electrolysis, as we detected two new products, acetate and pyruvate, and formate traces. This indicates that without dihydroxyacetone degradation it is impossible to obtain acetate and pyruvate, as well as lactate. Because of that, their presence in the final product distribution will highly depend on the experimental setup rather than the electrode performance. For this reason, we decided that they should be considered in conjunction with dihydroxyacetone.

2.5. Glycerol Electrolysis Coupled with CO_2 Reduction Reaction in a Continuous Flow Cell

Given the current limitations of the batch electrolysis setup, the electrodes were tested in a coelectrolysis setup in a flow cell at two different current densities, 90 and 200 mA cm^{-2}. The GOR was coupled with CO_2 reduction toward formate, employing a previously studied Bi/C catalyst as a gas diffusion electrode (GDE).[37]

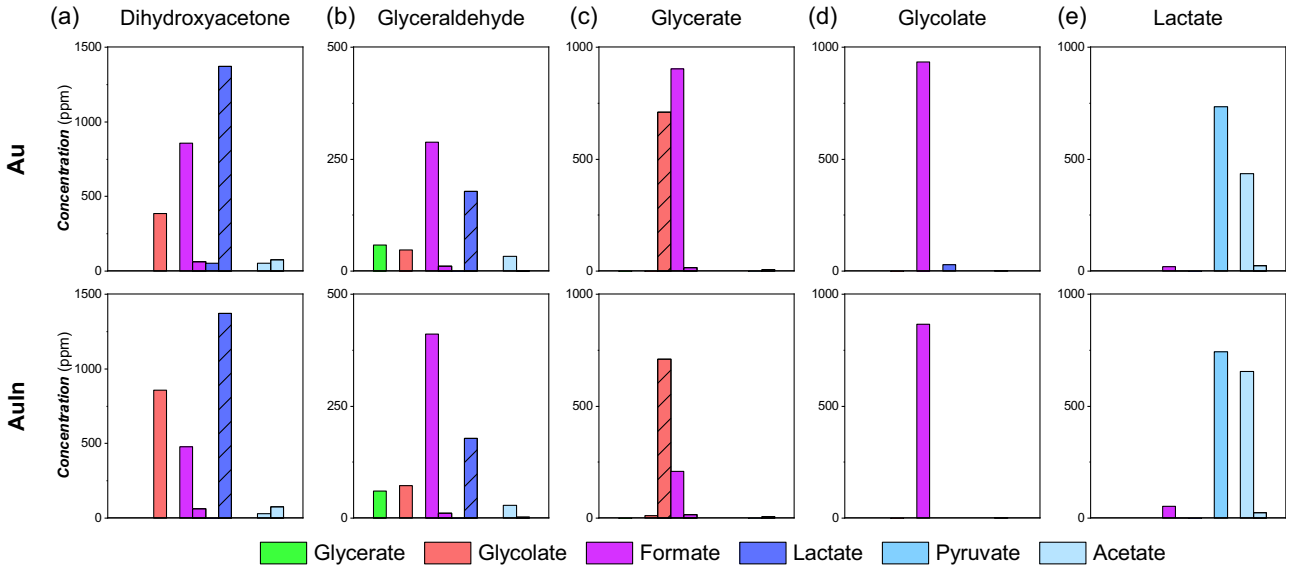

Figure 5. Anolyte composition (in ppm) of the divided cell electrolysis of 15 mL of KOH 1 M and a) dihydroxyacetone 0.1 M, b) glyceraldehyde 0.01 M, c) glycerate 0.1 M, d) glycolate 0.1 M, and e) lactate 0.1 M, at a current of 41.6 mA cm^{-2} and a charge of 10 C mL^{-1}. Stripped columns represent the chemically obtained products and full columns the electrochemically obtained products.

© 2025 The Author(s). ChemSusChem published by Wiley-VCH GmbH

1864564x, 2025, 12, Downloaded from https://chemistry-europe.onlinelibrary.wiley.com/doi/10.1002/cssc.202402378 by Universidad De Cantabria, Wiley Online Library on [07/07/2025]. See the Terms and Conditions (https://onlinelibrary.wiley.com/terms-and-conditions) on Wiley Online Library for rules of use; OA articles are governed by the applicable Creative Commons License

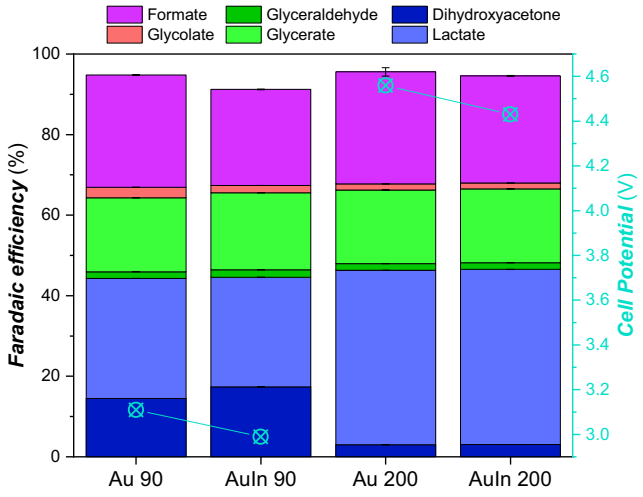

Figure 6. FE for glycerol oxidation and the corresponding cell potential in flow cell electrolysis at 90 and 200 mA cm^{-2}.

As illustrated in **Figure 6**, at 90 mA cm^{-2}, we obtained considerable GOR FE exceeding 90% in the anodic compartment, attributing the remaining <10% to overoxidation to CO_2. Unfortunately, since ion chromatography did not detect enough carbonate to quantify it, these values are not reported in this article.

In the cathodic compartment, the FE to formate were ≈80%, which aligns with previously reported values (**Table 1**). We found that the product distribution between the Au and AuIn electrodes was similar. This suggests that the products generated in the flow cell setup are more influenced by the electrolyte flow rate and the cell configuration rather than the electrode catalytic differences.

The three primary products of the oxidation were dihydroxyacetone and lactate (45%), formate (27%), and glycerate (18%) with trace amounts of glyceraldehyde (1.5%) and glycolate (1.5%). This product distribution differs significantly from that achieved in batch electrolysis. This is due to the fact that in the flow cell configuration, the electrolyte is continuously replaced, which limits the extent of product overoxidation. Direct oxidation products are therefore more prevalent. A comparison of the obtained products with those from batch electrolysis reveals a significant decrease in glycolate. This indicates that in the batch electrolysis it was produced as an overoxidation of dihydroxyacetone, and the small amount obtained in the flow cell is due to glycerate degradation. In contrast, the similar production of glycerate indicates that it is derived from direct glycerol oxidation. Finally, despite a reduction in formate, its FE remains sufficient, indicating that it may originate from both direct oxidation and overoxidation.

Regarding the 200 mA cm^{-2} electrolysis, we observe a decrease of dihydroxyacetone due to a higher percentage being degraded to lactate, which was increased proportionally. As explained in the previous section, since lactate is produced via the Cannizzaro rearrangement mechanism from dihydroxyacetone, the overall product distribution remains unchanged. This constant product distribution indicates that the electrocatalytic selectivity of both electrodes is dependent on the species residence time on the electrode surface rather than the current density. In the cathodic compartment, the FE of CO_2 to formate were ≈40%, remaining consistent with the previously reported values (Table 1).

Comparing both electrodes, while the product distribution remained unchanged, the cell voltage was observed to be lower for the AuIn electrode. At 90 mA cm^{-2}, there was a decrease from 3.11 to 2.99 V, and at 200 mA cm^{-2}, it decreased from 4.56 to 4.43 V. This indicates that by introducing indium into the gold electrode, we reduce the GOR potential. Comparing the cell voltage of the AuIn electrode with previously studied anodes in this flow cell setup (Table 1) reveals a reduction of 0.4 V on cell potential at 90 mA cm^{-2}. As a result of this reduction, we also decrease the energy consumption (EC), from 208 to 202 kWh $kmol^{-1}$. As we increase the current density to 200 mA cm^{-2}, the difference between the AuIn electrode and previous catalysts becomes more pronounced. In these conditions, both the cell voltage and the EC are significantly lower than previously reported data. The cell

Table 1. Comparison of the anolyte flow rate per geometric area (Qa/A), catholyte flow rate per geometric area (Qc/A), cell voltage, FE, and EC of different catalysts in flow cell conditions. Detailed setup description and calculations can be found in Supporting Information.

Sample	Current density [mA cm^{-2}]	Qa/A [mL min^{-1} cm^{-2}]	Qc/A [mL min^{-1} cm^{-2}]	Cell voltage [V]	Cathodic FE to formate [%]	EC [kWh $kmol^{-1}$]	Anodic FE [%]	DHA	LA	GLAD	GLA	AHA	FA
This work, Au	90	0.57	0.15	3.11	81	206	95	14	30	2	18	3	28
This work, AuIn	90	0.57	0.15	2.99	89	202	91	17	27	2	19	2	24
Ni-Co LDH[38]	90	1.71	0.15	3.40	83	219	99	7	0	21	16	0	55
Pt/C-PE/Bi_2O_3[39]	90	1.71	0.15	3.62	93	208	98	6	0	3	10	0	79
Pt/C-PE[40]	90	0.57	0.15	4.51	85	283	67	0	9	13	12	0	33
DSA-OER[41]	90	0.57	0.15	3.10	90	186	–	–	–	–	–	–	–
This work, Au	200	0.57	0.07	4.56	43	566	96	3	43	2	18	2	28
This work, AuIn	200	0.57	0.07	4.43	40	583	94	3	43	2	18	1	27
Pt/C-PE/Bi_2O_3[39]	200	1.71	0.07	6.91	41	900	39	3	0	7	3	0	26
Pt/C-PE[40]	200	1.71	0.07	6.94	39	936	28	1	1	2	1	0	23
DSA-OER[41]	200	0.57	0.07	4.50	45	535	–	–	–	–	–	–	–

© 2025 The Author(s). ChemSusChem published by Wiley-VCH GmbH

18645564x, 2025, 12, Downloaded from https://chemistry-europe.onlinelibrary.wiley.com/doi/10.1002/cssc.202402378 by Universidad De Cantabria, Wiley Online Library on [07/07/2025]. See the Terms and Conditions (https://onlinelibrary.wiley.com/terms-and-conditions) on Wiley Online Library for rules of use; OA articles are governed by the applicable Creative Commons License

voltage was reduced by 2.5 V, while the energy was decreased from 900 to 550 kWh $kmol^{-1}$.

Comparing the Au and AuIn catalysts with the previously studied ones in Table 1, we can see that in regard to the potential there is a major decrease in cell voltage compared to the other GOR electrocatalysts. In regard to the GOR, all electrodes exhibited high FE at 90 mA cm^{-2}, indicating minimal overoxidation to CO_2. It is noteworthy that at 200 mA cm^{-2}, the overall anodic FE for glycerol oxidation remained above 90%, which contrasts with the reduced efficiency observed on the Pt/C electrocatalyst at high current densities. Additionally, an analysis of the product distribution reveals notable differences between the AuIn and Au electrodes and the Ni-Co and Pt/C electrodes. This is because the previous catalysts promote formate production, whereas AuIn promotes the formation of C3 products such as dihydroxyacetone, lactate, and glycerate, which have a higher added value.

Although the AuIn electrode shows great advances compared to the other GOR catalysts, it should be noted that it has a very similar cell potential to the DSA-OER electrocatalyst. Considering DSA as a candidate electrocatalyst for GOR, the monitoring of the anode potential (Figure S7, Supporting Information) in the flow cell setup described in Figure S8, Supporting Information, shows that glycerol has no effect on the DSA electrode potential, while it induced a significant change in the NiCo and AuIn electrodes. In addition, DSA has poor glycerol conversion compared to the other electrocatalyst (Figure S9, Supporting Information), as it does not even reach 40% FE, since the GOR can be in direct competition with the OER. Therefore, the DSA electrode would not be suitable for glycerol covalorization, whereas the AuIn would be.

After electrolysis, postmortem characterization was performed to assess the stability of the electrodes. From FESEM images (Figure S10, Supporting Information), it can be seen that the morphology of both Au and AuIn remains largely unchanged. However, in some areas, small fragments of material have detached, showing signs of mechanical erosion. Additionally, EDS measurements (Table S6, Supporting Information) confirm that the AuIn composition has not changed significantly, indicating that the material has good chemical stability.

3. Conclusion

This work demonstrated the successful synthesis of a gold–indium alloy by electrodeposition on porous metal foams. The introduction of indium into gold resulted in a reduction of the catalyst cost by 28% and a transformation of the rough but plain gold structure into a cauliflower morphology, thereby increasing the electrode surface area by over 19 times. This new alloy also enhanced the electrocatalytic properties of gold for glycerol oxidation, exhibiting an onset potential of $0.62V_{RHE}$ compared to the $0.85V_{RHE}$ of the bare gold. This was demonstrated in flow cell glycerol electrolysis tests with a reduced cell potential and achieving total FE exceeding 90% while maintaining the product distribution at high current densities up to 200 mA cm^{-2}.

4. Experimental Section

Electrode Synthesis

The following materials were procured from Merck: analytical grade potassium cyanide (KCN), indium (III) sulfate ($In_2(SO_4)_3$, ≥98.0%), potassium hydroxide (KOH, 99.99%), acetone (C_3H_6O, 99.5%), and D-glucose ($C_6H_{12}O_6$, ≥99.5% (GC)). Sulfuric acid (H_2SO_4, 95%) was procured from Panreac. Potassium cyanurate (I) ($K[Au(CN)_2]$, 99%) was provided by Plating Decor Recubrimientos, S.L.

First, a 0.25 M indium (In^{3+}) precursor solution was prepared and adjusted to pH 2 using a diluted H_2SO_4 solution. The electrolyte was prepared in a 400 mL Pyrex jacketed cell, with the components added to DI water in the following order: 1M KCN, 0.1 M D-glucose, 0.05 M In^{3+} from the former precursor solution, 1.3 M KOH, and 0.025 M $K[Au(CN)_2]$. The electrodeposition process was conducted using a Princeton Applied Research VMP2 potentiostat with EC-Lab software, with the temperature maintained at 70 °C using a PolyScience thermostat. For each catalyst electrodeposition, a 16 cm^2 area of Ni-foam substrates (Recemat Ni-4753, 1.6 mm thick) was cleaned in acetone, rinsed with water, and then placed in the electrochemical cell as a working electrode. The counter electrode was a titanium iridium oxide mesh, while a saturated silver/silver chloride electrode was employed as the reference electrode. The electrodeposition of the Au–In electrode was conducted by applying a current density of -80 mA cm^{-2} for a duration of 120 s. For the electrodeposition of the Au electrode, a similar bath was utilized, except for the addition of D-glucose and $In_2(SO_4)_3$. To synthesize the electrodes, a current density of -70 mA cm^{-2} was applied for a duration of 120 s.

Characterization

The morphology of the Au and AuIn electrodes was analyzed using FESEM on a JEOL J-7100 coupled with EDS. XRD patterns were acquired using a PANalytical X'pert PRO diffractometer with monochromatized Cu Kα radiation ($\lambda = 1.5406$ Å) operating at 45 kV and 40 mA in a Bragg–Brentano configuration, and XPS spectra were recorded using an ESFOSCAN an equipment based on the PHI 5000 VersaProbe 4 from Physical Electronics (ULVAC-PHI), with monochromatized Al Kα radiation (1486.6 eV).

The electrochemical measurements were performed in a VSP biologic SA potentiostat with EC-Lab software in a conventional 3-electrode electrochemical cell. The Au and AuIn electrodes were the working electrode, a platinum filament the counter electrode, and a saturated silver/silver chloride electrode the reference electrode. The exposed geometric surface area was 1 cm^2, delimited by a Teflon tape. Surface roughness measurements were done in a 1 M KOH electrolyte, and cyclic voltammetry measurements were done in a 1 M KOH and 0.1 M glycerol electrolyte.

Batch Electrolysis and GOR Product Analysis

Potassium hydroxide (KOH, pa) was purchased from Supelco. Glycerol ($C_3H_8O_3$, 99.5%) and formic acid (99%) were purchased from VWR chemicals. Dihydroxyacetone (reagent grade) and glyceraldehyde (90%) were purchased from Merck. Lactic acid (LA, 90%) was purchased from Panreac. Glyceric acid (20% in water) was purchased from TCI. Glycolic acid (99%) was purchased from ACROS organics.

To determine the FE for glycerol oxidation, the experiments were carried out in a single-compartment electrochemical cell with 5 mL capacity, using 1 M KOH and 0.1 M glycerol as electrolyte solution. Au and AuIn electrodes were used as working electrode, a platinum filament as the counter electrode, and 1 mm leak-free Ag|AgCl (3.5 M KCl) reference electrode (Warner Instruments). A current of

© 2025 The Author(s). ChemSusChem published by Wiley-VCH GmbH

18645564x, 2025, 12, Downloaded from https://chemistry-europe.onlinelibrary.wiley.com/doi/10.1002/cssc.202402378 by Universidad De Cantabria, Wiley Online Library on [07/07/2025]. See the Terms and Conditions (https://onlinelibrary.wiley.com/terms-and-conditions) on Wiley Online Library for rules of use; OA articles are governed by the applicable Creative Commons License

18645564x, 2025, 12, Downloaded from https://chemistry-europe.onlinelibrary.wiley.com/doi/10.1002/cssc.202402378 by Universidad De Cantabria, Wiley Online Library on [07/07/2025]. See the Terms and Conditions (https://onlinelibrary.wiley.com/terms-and-conditions) on Wiley Online Library for rules of use; OA articles are governed by the applicable Creative Commons License

-41.6 mA cm^{-2} was applied until a charge of 25.7 C was achieved. Then, the electrolyte was neutralized with 0.14 mL of concentrated H_2SO_4 (95%) to acidify the solution and prevent dihydroxyacetone degradation. A single experiment was done for each condition. Then, the products were analyzed by high-performance liquid chromatography (HPLC) and H-NMR spectroscopy. For each product, the FE was calculated according to Equation (S1), Supporting Information.

HPLC analysis was conducted using a Waters Alliance e2695 cromatography with an Aminex HPLX-87H carboxylic acid column at 60 °C, with a sample loop of 100 μL. Diluted sulfuric acid (10 mM) was used as the mobile phase at a flow rate of 0.6 mL min^{-1}. The products were detected with a Jasco UV-1570 UV–vis spectrophotometer and a Waters 2414 refractive index detector. H-NMR analysis was carried out on a Bruker 400 instrument, with a water suppression method. For sample preparation, 490 μL of the electrolyte sample was mixed with 90 μL of deuterium oxide and 20 μL of 0.2%vol DMSO as an internal standard.

The electrolysis of glycerol oxidation products (dihydroxyacetone, glyceraldehyde, lactate, glycerate, glycolate, and formate) was conducted in a separated H-cell with two 15 mL compartments separated with a Nafion 117 membrane. Au and AuIn electrodes were used as working electrode, a platinum filament as the counter electrode, and a leak-free Ag|AgCl|KCl reference electrode. A current of 41.6 mA cm^2 was applied until a charge of 150 C was achieved. Then, the electrolyte was neutralized with 0.42 mL of concentrated H_2SO_4 (95%) to acidify the solution and prevent dihydroxyacetone degradation. A single experiment was done for each condition. Then, the products were characterized by H-NMR.

Continuous Flow Electrolysis Coupled with CO_2 *Reduction*

Potassium hydroxide (KOH, 85% purity, pharma grade), potassium chloride (KCl, pharma grade), and potassium hydrogen carbonate ($KHCO_3$, pharma grade) were purchased from PanReac AppliChem. Glycerol ($C_3H_8O_3$, 99%) was purchased from Sigma–Aldrich.

Flow cell electrolysis was done with the Au and AuIn electrode as the anode and a Bi/C-GDE cathode with a potentiostat-galvanostat (Arbin Instruments, MSTAT4). Both electrodes had an area of 10 cm^2 and were put in a continuous filter press electrochemical reactor following the schemes of Figure S11 and S12, Supporting Information. Two peristaltic pumps (Watson Marlow 320, Watson Marlow Group) were used to pump the electrolytes through the reactor. Additionally, a CO_2 gas flow of 200 mL$_n$ min^{-1} was supplied through the GDE. The anolyte consisted of an aqueous solution of 1.0 M KOH + 1.0 M glycerol, and the catholyte consisted of a 0.5 M KCl + 0.45 M $KHCO_3$ solution. All the experiments were conducted under ambient temperature and pressure conditions, similar to previous studies.[38–40] Different flow rates as well as current densities were tested as described in Table S7, Supporting Information. During the electrolysis, the cell potential was measured with a potentiometer at 15 min intervals. Two replicates were done for every electrolysis condition for a duration of 1 h each. Electrolyte aliquots were collected every 30 min, and the anodic samples were neutralized with concentrated H_2SO_4 (95%). Then, the cathodic products were analyzed by ion chromatography and the anodic products by HPLC and ion chromatography.

An Agilent 1100 series VWD chromatograph with an ion exchange column (Hi-Plex-H, 300 × 7.7 mm, Agilent) was used for HPLC analysis. The mobile phase consisted of a 94/6 v/v%, 5 mM H_2SO_4, and acetonitrile (Acetonitrile CHROMASOLVTM Plus, for HPLC ≥ 99.9%), at a flow rate of 0.6 mL min^{-1}, at 50 °C and with injection volume of 50 μL. The products were detected with a diode array detector. The ion chromatography analysis was conducted using a Dionex ICS system and an AS9-HC column. 4.5 mM Na_2CO_3 was used as the mobile phase at a 1 mL min^{-1} flow rate.[40] EC and FE in continuous flow electrolysis were calculated according to Equation (S8) and (S9), Supporting Information.

Acknowledgements

The authors gratefully acknowledge support through coordinated project CO2GLY (PID2022–138491OB-C33, PID2022–138491OB-C32, PID2022–138491OB-C31) funded by MICIU/AEI/10.13039/501100011033 and ERDF/EU. M.M. and M.A. are grateful to AGAUR-Generalitat de Catalunya for 2024 FI-1 00421 and 2021DI020 grants. The authors thank Centres Científics i Tecnologics (CCiTUB), Universitat de Barcelona, for the expert and technical help on XPS, HPLC, FESEM, and H-NMR techniques.

Conflict of Interest

The authors declare no conflict of interest.

Keywords: continuous CO_2 electroreduction · coupled electrolysis · foam-based anodes · glycerol electrooxidation · gold–indium electrocatalyst

[1] T. Attarbachi, M. D. Kingsley, V. Spallina, *Fuel* **2023**, *340*, 127485.
[2] S. Verma, S. Lu, P. J. A. Kenis, *Nat. Energy* **2019**, *4*, 466.
[3] J. Wu, X. Yang, M. Gong, *Chin. J. Catal.* **2022**, *43*, 2966.
[4] T. Li, D. A. Harrington, *ChemSusChem* **2021**, *14*, 1472.
[5] Y. Xu, T. Liu, K. Shi, H. Yu, K. Deng, Z. Wang, X. Li, L. Wang, H. Wang, *Chem. Commun.* **2023**, *59*, 1817.
[6] P. Wang, G. Wang, K. Chen, W. Pan, L. Yi, J. Wang, Q. Chen, J. Chen, Z. Wen, *Nano Energy* **2023**, *118*, 108992.
[7] G. Li, T. Yan, X. Chen, H. Liu, S. Zhang, X. Ma, *Energy Fuels* **2022**, *36*, 4234.
[8] D. Xu, K. Li, B. Jia, W. Sun, W. Zhang, X. Liu, T. Ma, *Carbon Energy* **2023**, *5*, e230.
[9] Y. Zang, P. Wei, H. Li, D. Gao, G. Wang, *Electrochem. Energy Rev.* **2022**, *5*, 29.
[10] J. Na, B. Seo, J. Kim, C. W. Lee, H. Lee, Y. J. Hwang, B. K. Min, D. K. Lee, H.-S. Oh, U. Lee, *Nat. Commun.* **2019**, *10*, 5193.
[11] J. R. C. Junqueira, D. Das, A. Cathrin Brix, S. Dieckhöfer, J. Weidner, X. Wang, J. Shi, W. Schuhmann, *ChemSusChem* **2023**, *16*, e202202349.
[12] K. Jiang, Z. Li, Z. Zhang, J. Li, X. Qi, J. Zhou, X. Wang, H. Wei, H. Chu, *Inorg. Chem.* **2023**, *62*, 8145.
[13] Y. Wang, W. Liu, J. Zhao, Z. Wang, N. Zhao, *Appl. Catal., A* **2024**, *671*, 119578.
[14] Y.-H. Ke, H.-Y. Qin, X. Wang, H. Li, H. Liu, H. Yuan, *J. Porous Mater.* **2023**, *30*, 723.
[15] D. Kim, L. S. Oh, Y. C. Tan, H. Song, H. J. Kim, J. Oh, *ACS Catal.* **2021**, *11*, 14926.
[16] Y. Yan, P. Hao, Y. Fu, W. Chen, Q. Shi, H. Zhou, X. Kong, Z. Li, M. Shao, X. Duan, *AIChE J.* **2024**, *70*, e18370.
[17] R. Oh, X. Huang, X. Lu, C. Chen, Y.-Y. Lou, L. Geng, X. Zhang, D. Du, J. Li, W. Yan, G.-S. Park, O. Akdim, S. K. Kim, S.-G. Sun, *ACS Sustainable Chem. Eng.* **2023**, *11*, 11681.
[18] M. Frutis-Murillo, I. Velázquez-Hernández, R. Esparza, J. E. López-Meza, N. Cayetano-Castro, G. Rosas, *Appl. Surf. Sci.* **2024**, *642*, 158628.
[19] Z. Wang, Q. Hong, B. Miao, T. Wang, Y. Ding, P. Jin, P. Chen, Y. Chen, *Chin. Chem. Lett.* **2024**, *35*, 108458.
[20] Y. Yan, Q. Wang, P. Hao, H. Zhou, X. Kong, Z. Li, M. Shao, *ACS Appl. Mater. Interfaces* **2023**, *15*, 23265.
[21] S. Prasad Nayak, L. K. Ventrapragada, A. M. Rao, J. K. Kiran Kumar, *Mater. Lett.* **2023**, *330*, 133212.
[22] Y. Xie, L. Sun, X. Pan, Z. Zhou, Y. Zheng, X. Yang, G. Zhao, *Carbon* **2023**, *203*, 88.
[23] C. Dai, L. Sun, H. Liao, B. Khezri, R. D. Webster, A. C. Fisher, Z. J. Xu, *J. Catal.* **2017**, *356*, 14.
[24] T. R. Maumau, R. M. Modibedi, M. K. Mathe, *Mater. Today: Proc.* **2018**, *5*, 10542.

© 2025 The Author(s). ChemSusChem published by Wiley-VCH GmbH

[25] M. S. E. Houache, A. Shubair, M. G. Sandoval, R. Safari, G. A. Botton, P. V. Jasen, E. A. González, E. A. Baranova, *J. Catal.* **2021**, *396*, 1.
[26] N. Tuleushova, A. Amanova, I. Abdellah, M. Benoit, H. Remita, D. Cornu, Y. Holade, S. Tingry, *Nanomaterials* **2023**, *13*, 1713.
[27] H. You, F. Gao, C. Wang, T. Song, J. Li, X. Wang, Y. Zhang, Y. Du, *ChemElectroChem* **2021**, *8*, 3637.
[28] Z. Lu, L. Zou, W. Song, *Molecules* **2023**, *28*, 1502.
[29] S. Yin, S. Liu, Z. Wang, Y. Xu, X. Li, H. Wang, L. Wang, *Chem. Eng. J.* **2022**, *435*, 134711.
[30] L. Pérez-Martínez, L. Balke, A. Cuesta, *J. Catal.* **2021**, *394*, 1.
[31] C. C. Lima, M. V. F. Rodrigues, A. F. M. Neto, C. R. Zanata, C. T. G. V. M. T. Pires, L. S. Costa, J. Solla-Gullón, P. S. Fernández, *Appl. Catal., B* **2020**, *279*, 119369.
[32] S. Lux, *Chem. Biochem. Eng. Q.* **2016**, *29*, 575.
[33] V. A. Yaylayan, S. Harty-Majors, A. A. Ismail, *Carbohydr. Res.* **1999**, *318*, 20.
[34] L. Cheng, C. Doubleday, R. Breslow, *Proc. Natl. Acad. Sci. U.S.A.* **2015**, *112*, 4218.
[35] Y. Kwon, K. J. P. Schouten, M. T. M. Koper, *ChemCatChem* **2011**, *3*, 1176.
[36] C. H. Lam, A. J. Bloomfield, P. T. Anastas, *Green Chem.* **2017**, *19*, 1958.
[37] G. Díaz-Sainz, M. Alvarez-Guerra, B. Ávila-Bolívar, J. Solla-Gullón, V. Montiel, A. Irabien, *Chem. Eng. J.* **2021**, *405*, 126965.
[38] K. Fernández-Caso, M. Molera, T. Andreu, J. Solla-Gullón, V. Montiel, G. Díaz-Sainz, M. Álvarez-Guerra, A. Irabien, *Chem. Eng. J.* **2024**, *480*, 147908.
[39] A. Peña-Rodríguez, K. Fernández-Caso, G. Díaz-Sainz, M. Álvarez-Guerra, V. Montiel, J. Solla-Gullón, *ACS Sustainable Chem. Eng.* **2024**, *12*, 3671.
[40] K. Fernández-Caso, A. Peña-Rodríguez, J. Solla-Gullón, V. Montiel, G. Díaz-Sainz, M. Alvarez-Guerra, A. Irabien, *J. CO2 Util.* **2023**, *70*, 102431.
[41] G. Díaz-Sainz, M. Alvarez-Guerra, J. Solla-Gullón, L. García-Cruz, V. Montiel, A. Irabien, *J. CO2 Util.* **2019**, *34*, 12.

Manuscript received: November 4, 2024
Revised manuscript received: February 25, 2025
Version of record online: April 10, 2025

© 2025 The Author(s). ChemSusChem published by Wiley-VCH GmbH

1864564x, 2025, 12, Downloaded from https://chemistry-europe.onlinelibrary.wiley.com/doi/10.1002/cssc.202402378 by Universidad De Cantabria, Wiley Online Library on [07/07/2025]. See the Terms and Conditions (https://onlinelibrary.wiley.com/terms-and-conditions) on Wiley Online Library for rules of use; OA articles are governed by the applicable Creative Commons License